Cerâmica. 2026, v.72:eEXOX2464 http://dx.doi.org/10.1590/EXOX2464
ARTICLE

Evaluation of the Photocatalytic Performance of TiO_2 Modified Mortars Applied to Building Facades

V. A. S. Ribeiro, A. F. Oliveira, V. C. Santos*, L. P. Silva, C. H. C. Carvalho
Federal University of Itajubá, BPS Avenue, 1303, Itajubá-MG, Brazil

Abstract

This study developed and characterized photocatalytic coating mortars incorporating titanium dioxide (TiO_2) and evaluated their efficiency in pollutant degradation and environmental impact. Mortar mixtures containing 0%, 2%, 4%, 6%, and 10% TiO_2 by cement weight were analyzed with respect to structural, microstructural, and photocatalytic properties. Performance was assessed through methylene blue degradation under UV light, supported by UV–Vis spectrophotometry, SEM, and XRD analyses. The results showed that higher TiO_2 concentrations enhanced photocatalytic efficiency, particularly in the degradation of organic compounds. It was concluded that the developed mortars exhibit strong potential for application on urban building facades, offering benefits such as self-cleaning capability, reduced maintenance costs, and improved air quality, thereby contributing to sustainability in the construction sector.
Keywords: Photocatalysis; Titanium dioxide (TiO_2); Building facades; Air purification; Sustainability; Self-cleaning coatings.

INTRODUCTION

In recent decades, social and environmental transformations have driven the development of more sustainable, durable, and lower-maintenance building materials. In this context, photocatalytic cementitious materials have emerged as an innovative solution to reduce urban pollution, improve the durability of buildings, and decrease operational costs related to the maintenance and cleaning of exposed surfaces [1]. These materials can decompose harmful organic and inorganic compounds through heterogeneous photocatalysis processes activated by sunlight or ultraviolet radiation [2].

The self-cleaning characteristic can be applied to various types of surfaces, encompassing both building construction elements and movable objects, such as streetlights and vehicles. This functionality is made possible by the use of photocatalytic materials, whose principle of action is based on photocatalysis—a process in which light radiation strikes a catalytic compound, accelerating chemical reactions without consuming it [3,4].

According to Fontolan et al. (2023) [1], photocatalysis allows the degradation of atmospheric pollutants, such as sulfur oxides (SO_x), nitrogen oxides (NO_x), and volatile organic compounds (VOCs), transforming them into inert substances. Furthermore, in the presence of a photocatalyst, they exhibit hydrophilic behavior, favoring the formation of a water film that runs down vertical surfaces during precipitation events, passively removing impurities. Initially applied to smooth surfaces, this technology is also being incorporated into concrete and mortars, promoting a self-cleaning effect in external building components where there is high exposure to solar radiation and rainwater [6].

Building facades often darken and change color over time, requiring frequent and costly maintenance. The application of photocatalytic materials reduces the need for cleaning, contributes to improved air quality, and has an antibacterial effect [7]. Studies also indicate that, depending on the type of paint and pigmentation, even graffiti can be degraded by the photocatalytic effect.

Photocatalytic materials are mostly semiconductors, with titanium dioxide (TiO_2) being the most widely used, especially due to its efficient activation by ultraviolet (UV) radiation. Among the available photocatalysts, titanium dioxide (TiO_2), particularly in the anatase, rutile, and brookite phases, has been extensively studied and applied due to its exceptional properties: high photocatalytic efficiency, chemical stability, low cost, and non-toxicity. The mechanism of action is based on electronic excitation when TiO_2 is irradiated with light of wavelength less than 387 nm, promoting the formation of electron-hole pairs (e^-/h^+). These charge carriers, when interacting with adsorbed molecules such as oxygen and water, generate highly reactive species, such as hydroxyl radicals (•OH) and superoxide anions ($O_2^{\bullet-}$), capable of oxidizing and decomposing organic and inorganic contaminants [6].

The incorporation of TiO_2 nanoparticles into cementitious matrices, such as mortars and concretes, seeks to exploit these properties, giving the materials self-cleaning and self-decontaminating characteristics. Recent research shows that the controlled addition of TiO_2 not only promotes the degradation of pollutants but can also improve certain physical properties of the matrix, such as density and resistance to water penetration, although negative effects on mechanical properties may occur depending on the dosage and dispersion of the nanomaterial. [8].

**valquiria@unifei.edu.br*
https://orcid.org/0000-0001-7744-3262

In the field of civil engineering and materials, the use of TiO_2 in self-cleaning coatings has been increasingly explored, especially in European and Asian countries, where there are more restrictive environmental laws and a growing demand for sustainable construction [2].

One of the most established methods for evaluating the photocatalytic activity of these materials is the degradation of methylene blue (MB) dye in aqueous solution under ultraviolet radiation.

This experimental model stands out for its simplicity, ease of spectrophotometric monitoring, and good correlation with the degradation activity of more complex compounds [9].

Recently, studies have demonstrated the effectiveness of this model in characterizing cementitious materials modified with TiO_2, showing that the efficiency of the process strongly depends on the mass fraction of TiO_2, the specific surface area of the particles, and the porosity of the matrix [10].

Furthermore, recent research highlights the importance of fundamental parameters, such as the homogeneous dispersion of the photocatalyst in the cementitious matrix and the type of chemical and physical interaction between TiO_2 and the cement components, to maximize the photocatalytic efficiency of the materials.

Uniform dispersion of TiO_2 is essential to ensure that the active particles are evenly distributed on the surface and inside the mortar or concrete, preventing clumping that reduces the contact area with UV radiation and pollutants. Similarly, the type of bond established between TiO_2 and the hydration products of cement, such as calcium hydroxide (CH) and hydrated calcium silicate (C–S–H), directly influences the stability of the photocatalyst in the matrix and the efficient transfer of charges during oxidation and reduction reactions.

Thus, controlling these factors contributes to the durability, photocatalytic activity, and self-cleaning performance of the material, which are crucial aspects in the development of cementitious surfaces with advanced functionalities. The combination of traditional mortar preparation techniques with nanoparticle functionalization processes or TiO_2 surface modifications has shown promising results in increasing photocatalytic efficiency [11].

In this context, the present work aims to prepare self-cleaning mortars by incorporating different mass fractions of TiO_2, in order to evaluate the influence of this variable on the photocatalytic efficiency of the material.

METHODOLOGY

For the preparation of the coating mortar with photocatalytic properties, the following materials were used: fine aggregate composed of washed natural sand; titanium dioxide from the VETEC brand by SIGMA-ALDRICH BRASIL LTDA; Portland cement type CP II-F 32, from the CSN brand, in accordance with [12]; potable water for mixing the mixture, HP Ultra metakaolin, and ADI-SUPER H24 plasticizing additive from the Aditibras brand. The fine aggregate used in this study is natural sand, mainly composed of quartz (SiO_2), with minor amounts of feldspar and other minerals, which is characteristic of conventional fine aggregates used in construction materials.

The determination of the specific gravity of the fine aggregate was carried out according to the procedures established by the [13] standard. The value obtained for the specific gravity of the fine aggregate was 2.62 g/cm³, meeting the normative criteria for the characterization and analysis of aggregates.

NBR 16605 (2017) [14] standard was adopted, ensuring accuracy and reproducibility in the results. This standard prescribes a method based on the use of a volumetric flask (such as the Le Chatelier flask). The value obtained for the cement was 2.80 g/cm³, meeting the normative criteria for characterization and analysis of Portland cement.

For the production of the photocatalytic mortar, a 1:3 mix by volume was adopted, corresponding to a proportion of Portland cement and sand. During the preparation of the mixture, different concentrations of titanium dioxide (TiO_2) were incorporated, corresponding to 0% (reference), 2%, 4%, 6%, and 10% in relation to the mass of cement.

The mixture was used to mold samples with dimensions of 5 cm x 5 cm x 1 cm for characterization using a UV-Vis spectrophotometer. The material was carefully homogenized in each composition, ensuring the uniform distribution of titanium dioxide (TiO_2) in the mortar matrix. The consumption of materials used in molding the samples, as well as the corresponding water/cement ratio, was determined according to the consistency recommended by the standard and is presented in Table I.

The samples were subjected to a wet curing process for 28 days in order to guarantee stability and the full development

Table I - Consumption of materials used.

Content (%)	Cement (g)	Sand (g)	Water (ml)	TiO_2 (g)	Metakaolin (g)	Plasticizing Additive (mL)	a/c ratio
0	12.5	37.5	6.25	0.00	1.25	0.375	0.5
2	12.5	37.5	6.25	0.25	1.25	0.375	0.5
4	12.5	37.5	6.25	0.50	1.25	0.375	0.5
6	12.5	37.5	6.25	0.75	1.25	0.375	0.5
10	12.5	37.5	6.25	1.25	1.25	0.375	0.5

Table II - Conditions and exposure times in the solution in relation to the mortar and UV light.

Time	Features
0 min	This represents the initial absorbance of the dye without interaction with the coating mortar or exposure to UV light, used as a reference to characterize the initial absorbance of the solution.
30 min	This refers to the solution in contact with the coating mortar, but without exposure to UV light, serving as a control to evaluate degradation not activated by TiO□ (Adsorption).
60 min	It indicates the solution in contact with the coating mortar under UV light, marking the beginning of the photocatalytic degradation process mediated by titanium dioxide (TiO_2).
90 min	It represents the solution in continuous contact with the coating mortar under UV light, highlighting the progression of the photocatalysis process.
120 min	It represents the solution in continuous contact with the coating mortar under UV light, highlighting the progression of the photocatalysis process.
150 min	It represents the solution in continuous contact with the coating mortar under UV light, highlighting the progression of the photocatalysis process.
180 min	It represents the solution in continuous contact with the coating mortar under UV light, highlighting the progression of the photocatalysis process.

of the necessary properties. The curing process of the coating mortar was based on the applicable standards of ABNT NBR 13279 (1995) [15] and ABNT NBR 13749 (2013) [16].

After the curing process, the samples were previously dried at room temperature to ensure the elimination of residual moisture without significant structural changes for the photocatalysis test, X-ray characterization, scanning electron microscopy (SEM), and EDS.

The photocatalysis test was conducted using a Kasvi K37-UV-VIS spectrophotometer to evaluate the photocatalytic performance of a coating mortar incorporating titanium dioxide (TiO_2). The study consisted of monitoring the degradation of methylene blue over time, with the aim of characterizing the material's efficiency in removing the contaminant under controlled conditions. Initially, a solution of methylene blue dye was prepared with distilled water at a concentration of 0.005 g^{l-1}.

The experimental setup was carried out inside a specially constructed photocatalytic chamber, isolated from ambient light and with control of the experimental variables. The external structure of the chamber, made of wood, was internally lined with aluminum foil to reflect and uniformly distribute the UV light emitted by the lamps installed inside. The photocatalytic experiments were conducted using a UV-C lamp (45 cm in length and 2.6 cm in diameter), with a maximum emission peak at 254.7 nm and a power output of 15 W, positioned at a distance of 30 cm from the sample, with an exposure time of 3 h. These details were added to improve the reproducibility of the results and to better define the experimental conditions.

The recirculation of the methylene blue solution, directing the liquid directly over the surface of the mortar sample, was carried out using a pumping system, simulating real flow conditions and optimizing the contact between the dye and the photocatalytic surface.

The curves obtained represented different conditions and exposure times in the solution in relation to the mortar and UV light, allowing the evaluation of the photocatalytic system's behavior, as shown in Table II.

SEM images were obtained at different magnifications, allowing observation of surface characteristics such as particle distribution and the presence of TiO_2 agglomerates. In parallel, EDS was performed for qualitative analysis of the chemical elements present, verifying the uniformity of titanium dioxide incorporation in the mortar matrix.

The identification of crystalline phases was performed using X-ray diffraction (XRD) to determine the predominant crystalline phase in the analyzed material. The test was conducted using a Philips X'Pert MPD diffractometer, operating under conditions of 40 kV and 40 mA, with CuKα radiation. Angle scanning (2θ) was performed in the range

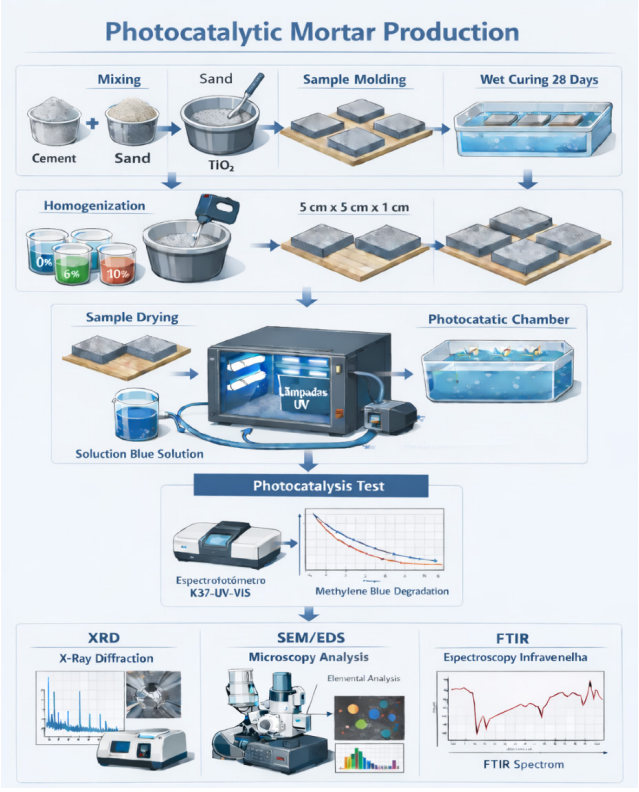

Figure 1: The diagram provides a clear and reproducible overview of the experimental procedure.

of 5° to 80°, with a step speed of 0.02°/s and an acquisition time of 1 s per step. The analysis of the crystalline phases was conducted using the X'Pert HighScore software, utilizing the reference standards available in the International Centre for Diffraction Data (ICDD) archives.

Spectroscopic characterization in the infrared region aims to identify and monitor the chemical bonds and functional groups present in the cementitious matrix and to evaluate possible interactions between TiO_2 and the mortar constituents. FTIR analysis was performed directly on the film samples using the Attenuated Total Reflectance (ATR) mode, without additional sample preparation. The spectra were recorded in the range of 600–4000 c^{-1}, with 12 scans, ensuring adequate spectral quality and reproducibility of the results. Figure 1 illustrates the experimental procedure, providing a clear and reproducible representation of the methodology employed.

The degradation efficiency (DE), which quantifies the proportion of contaminant removed from the solution during the degradation process, was calculated as follows:

$$DE(\%)=\frac{C_i - C_t}{C_i} x100 \quad (A)$$

where:
• DE (%) is the degradation efficiency,
• C_i is the initial concentration of the dye in the solution (mol/L or g/L).
• C_t is the concentration of the dye at time t (mol/L or g/L).

The degradation kinetics are also an important parameter for understanding how contaminant degradation occurs throughout the degradation process. In this case, the degradation kinetics is represented by the first-order mathematical model, given by:

$$\ln\frac{C_0}{C_t} = kt \quad (B)$$

Where k is the pseudo-first-order rate constant, expressed in min^{-1}, and et represents the time elapsed since the beginning of the photocatalytic process.

RESULTS AND DISCUSSIONS

Table III presents the particle size distribution values of the fine aggregate, indicating the cumulative percentage retained on each sieve and the corresponding passing fraction. The particle size analysis allowed the calculation of the fineness modulus (FM), an essential parameter for classifying the aggregate according to the ABNT NBR7211 (2022).

It was observed that there was no retention on the 6.30 mm and 4.80 mm sieves, indicating the absence of coarse particles and confirming that the material is entirely composed of fine grains, as expected for sand intended for the production of mortars and concretes.

The largest retained fraction was observed on the 0.60 mm sieve, totaling 987.01 g, corresponding to 88.31% of the total mass analyzed. This data reveals that most of the aggregate is concentrated in this particle size range.

Adding the retentions in the immediately superior and inferior sieves, it is found that approximately 98.64% of the material is between 1.20 mm and 0.30 mm, which characterizes a well-defined and cohesive distribution.

The cumulative passing percentage shows that 91.69% of the material passes through the 0.60 mm sieve, indicating a predominance of smaller diameter particles.

On the other hand, the percentage passing through the 0.15 mm sieve is only 0.68%, indicating a low content of very fine material (below 0.15 mm). These results suggest that the aggregate has a low quantity of fines, contributing to better workability and lower water demand in cementitious mixtures.

The fineness modulus (FM) value determined for the fine aggregate was 2.88. According to the ABNT NBR7211 (2022) [17] standard, this value falls within the range that

Table III - Particle size distribution of fine aggregate

# Sieve (mm)	Mass Retained (g)	% Retained	Cumulative % Retained	% passer
6.30	0	0.00	0.00	100
4.80	0.00	0.00	0.00	100
2.40	0.23	0.02	0.02	99.98
1.20	14.93	1.34	1.36	98.64
0.60	987.01	88.31	89.67	10.33
0.30	88.70	7.94	97.61	2.39
0.15	19.16	1.71	99.32	0.68
Bottom	7.58	0.68	100	0.00
∑	1117.61	100		
Specific gravity of aggregate (g/cm³)	1.66	Fineness modulus:		2.88
		Maximum Diameter (mm)		1.2

classifies the fine aggregate as medium sand, with the classification range being between 2.4 < FM < 3.3.

This value is close to the upper limit of this classification (2.88), indicating the significant presence of slightly coarser particles within the medium sand spectrum. This characteristic favors the packing of the grains and, consequently, improves the properties of the cementitious compound.

Based on the data presented in Table III, the maximum diameter of the particle size distribution was determined to be 1.2 mm, according to the criterion that establishes that this value must correspond to a cumulative retention percentage of less than 5%.

This demonstrates that, even in the upper ranges, the particles remain at sizes suitable for applications in rendering mortars. Furthermore, the specific gravity of the aggregate was determined to be 2.62 g/cm³, a value consistent with predominantly siliceous natural sands, used as a fundamental parameter for the material dosage calculations.

Thus, the results of the particle size analysis indicate that the fine aggregate has a well-distributed curve, with a predominance of medium particles, a low content of fines, and a maximum diameter compatible with the technical requirements for its application in cementitious elements.

The particle size distribution of the fine aggregate (natural sand) was determined by means of a sieving test, according to the procedures established in the ABNT NBR7211 (2022) [17] standard, and is represented in Figure 2.

The particle size distribution curve obtained for the fine aggregate is represented by the dashed line and describes the cumulative retained percentage as a function of the sieve opening. The curve indicates that the material is entirely contained between the zones called "lower and upper usable" and "lower and upper optimum," which demonstrates that the particle size distribution meets the normative limits for use in mortars and concretes.

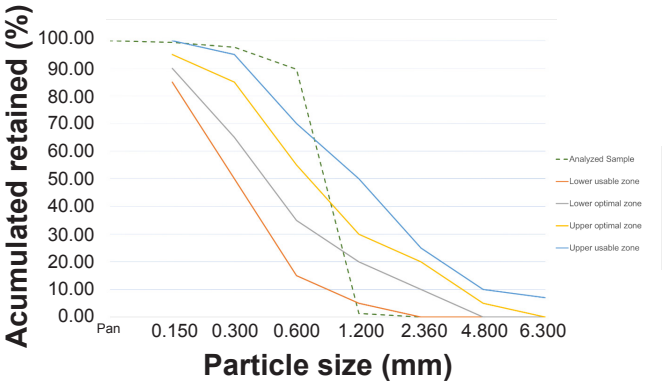

Figure 2: Particle size distribution curve of fine aggregate.

It is noted that the curve is positioned mostly between the upper optimum zone and the upper usable zone, indicating a predominance of medium to slightly coarser particles.

The absence of retention in the 6.30 mm and 4.80 mm sieves confirms the absence of coarse particles, reinforcing the classification of the aggregate as sand. The highest concentration of material occurs in the 0.60 mm sieve, based on the previous table, which recorded approximately 88.31% of the total mass in this range, revealing a well-defined and cohesive distribution with few fine particles. Furthermore, the curve is continuous and smooth, without abrupt discontinuities between the sieves, which characterizes a well-graded aggregate.

Figure 3 presents the X-ray diffraction (XRD) analysis, through which the crystallographic phases present in the mortars with different TiO_2 contents 0%, 2%, 4%, 6% and 10% TiO_2 by cement weight, were identified.

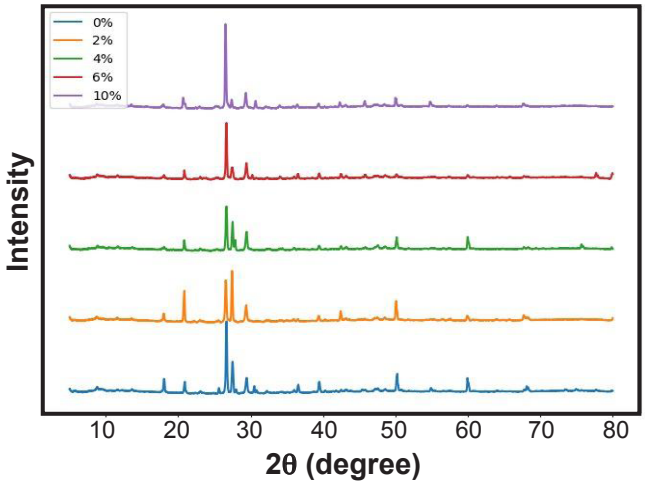

Figure 3: Infrared spectrum for mortars with TiO_2.

In the sample without TiO_2 (0%), the peaks are dominated by the characteristic phases of the cementitious matrix, with emphasis on SiO_2 (mainly associated with the aggregate), $CaCO_3$ (resulting from the carbonation of the cement and the presence of limestone), as well as C_3S and aluminosilicate phases. This diffractogram establishes the reference profile of the mortar without additions.

With the incorporation of 2% TiO_2, the appearance of the rutile phase (TiO_2) is clearly observed, in addition to the persistence of the SiO_2 and $CaCO_3$ phases. The presence of this phase indicates that, even at low concentrations, titanium oxide is incorporated in a crystalline form and is detectable by XRD.

A slight change in the relative intensity of the C_3S peaks is also noted, suggesting partial interaction of the additive with the calcium silicates.

In the sample with 4% TiO_2, rutile remains detectable, although with a lower relative intensity compared to 2%, which may be associated with greater dispersion of TiO_2 in the cementitious matrix or peak overlap. The SiO_2 and $CaCO_3$ phases continue to be predominant, but the evident absence of C_3S in this analysis suggests that the increase in TiO_2 content may be contributing to a modification of the hydrated clinker crystallization or to phase overlap in nearby regions of the diffractogram.

The transition becomes clearer in the sample with 6% TiO_2, in which, in addition to SiO_2 and $CaCO_3$, brookite (TiO_2) is present, a less stable polymorphic phase but of

greater photocatalytic interest. This result suggests that increasing the concentration favors the detection of new TiO_2 phases, indicating that part of the material may be crystallizing in different polymorphic forms. Furthermore, the calcium silicate phase ($CaSiO_3$) appears related to the hydration products of cement.

In the sample with 10% TiO_2, the evolution is even more evident. The diffractogram shows the coexistence of brookite, SiO_2, $CaCO_3$, and Ca $(OH)_2$, the latter typical of Portland cement hydration, in addition to the presence of aluminosilicates and aluminum sulfate-hydroxide. This diversity of phases suggests that the high TiO_2 content not only intensifies the presence of its polymorphs but also influences the hydration and crystallization of secondary compounds in the cement.

Figure 4 shows the infrared (FTIR) spectra of mortars containing different levels of TiO_2. This analysis allows the identification of the main functional groups present in the cementitious matrix and the verification of possible chemical interactions between titanium dioxide and the compounds formed during the cement hydration process.

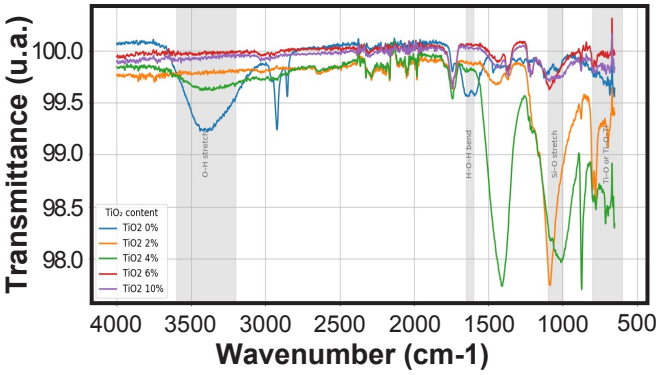

Figure 4: Infrared spectrum for mortars with TiO_2.

In the region between 3600–3200 cm^{-1}, a broad band related to O–H stretching is observed, attributed to the presence of hydroxyl groups originating from the water of hydration and the formation of calcium hydroxides (Ca $(OH)_2$). The intensity of this band tends to vary slightly with increasing TiO_2 content, suggesting the influence of the photocatalytic additive on water retention or the formation of hydrated products.

At around 1650 cm^{-1}, a band associated with the H–O–H deformation vibration is identified, also related to water physically adsorbed on the surface of the hydration products.

The bands located between 1000 and 900 cm^{-1} correspond to the Si–O–Si and Si–O stretching vibrations, typical of hydrated calcium silicates (C–S–H), which are mainly responsible for the mechanical strength of mortar. Small variations in the intensity and position of these bands indicate that TiO_2 may act in modifying the structure of the hydration products.

In the range close to 700–500 cm^{-1}, the appearance or increase in intensity of a characteristic Ti–O–Ti stretching band is observed, confirming the presence of titanium dioxide in the matrix. This band becomes more evident in samples with 6% and 10% TiO_2 contents, which confirms the progressive incorporation of the photocatalytic material.

In general, FTIR results indicate that the addition of TiO_2 does not significantly alter the main chemical structure of the cementitious matrix, but promotes surface interactions that may contribute to the stability of hydration products and potentially improve the photocatalytic performance of mortars.

In the spectra presented, metakaolin mainly influences the regions associated with Si–O and Al–O vibrations; that is, it appears indirectly in the graph bands. The 1000–900 cm^{-1} range (Si–O–Si and Si–O–Al stretch) is the region most affected by the presence of metakaolin. Metakaolin is rich in amorphous silicon (Si) and aluminum (Al), and during cement hydration, it reacts with calcium hydroxide ($Ca(OH)_2$), forming hydrated calcium silicates and aluminates (C–S–H and C–A–H) [19].

Figure 5 shows the absorbance spectra (α, in arbitrary units) as a function of wavelength (λ, in nm) for mortar samples without the addition of TiO_2 (0%) e (2%), over different exposure times (Reference, 30 min, 1h, 1h 30 min, 2h, 2h 30 min and 3h) during the photocatalysis test with methylene blue.

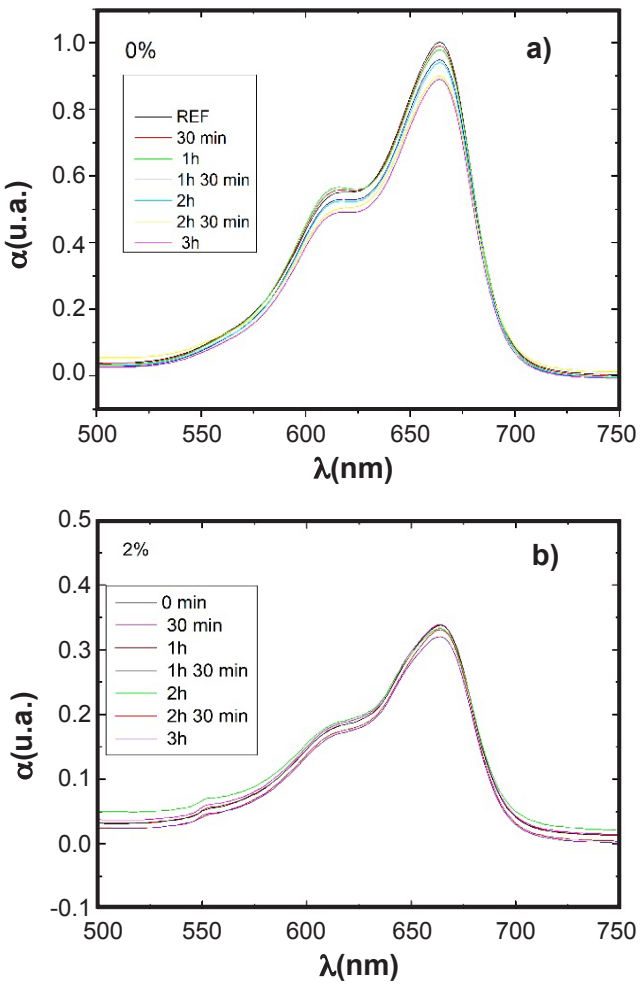

Figure 5: Absorbance spectra of mortar containing 0% and 2% TiO_2 by cement weight, obtained after different exposure times to ultraviolet radiation.

It is observed that all curves show a well-defined absorbance peak near 665 nm, characteristic of the methylene blue dye used as a marker of photocatalytic activity. Throughout the different exposure times, no significant reduction in the intensity of this peak is noted, indicating that the dye concentration remained practically constant throughout the test. This stability in the curves suggests that the mortar without TiO_2 does not possess appreciable photocatalytic activity.

The absence of variation in absorbance over time confirms that there was no effective degradation of methylene blue under UV irradiation, a behavior expected in materials without photocatalytic properties.

Therefore, the results obtained with the sample containing 0% TiO_2 serve as a control in the experiment, allowing direct comparisons with samples modified with different TiO_2 contents.

It is observed that all curves show a pronounced peak around 665 nm, which corresponds to the characteristic absorption band of methylene blue dye. However, unlike the sample with 0% TiO_2, in this case, there is a progressive reduction in the intensity of the absorbance peak as the exposure time to UV radiation increases. This decrease in absorbance over time shows that the dye is being gradually degraded, indicating that the mortar sample with 2% TiO_2 has effective photocatalytic activity.

Figure 6 shows the absorbance spectra (α, in arbitrary units) as a function of wavelength (λ, in nm) for a mortar sample with 4% e 6% TiO_2, subjected to UV radiation for different times: 0, 30 minutes, 1h, 1h30min, 2h, 2h30 min, and 3h.

The absorbance spectra obtained for mortars containing 4% TiO_2 subjected to UV radiation for different periods of time show evidence of the occurrence of the photocatalytic process. It is observed that the intensity of the main absorption band decreases progressively as the exposure time increases, indicating the continuous degradation of the organic compound present on the surface of the mortar.

It is observed that the degradation rate tends to decrease, which may be related to the decrease in pollutant concentration, the formation of intermediate byproducts that compete for active sites, or even limitations in mass transport within the cementitious matrix [20].

The absorbance spectra of mortar containing 6% TiO_2 subjected to UV radiation reveal a significant drop in the intensity of the main peak, located around 660 nm, when compared to the initial absorbance of the dye without interaction with the coating mortar or exposure to UV light, used as a reference to characterize the initial absorbance of the solution.

With increasing irradiation time (1 to 3 h), the decrease in absorbance continues, although at a lower intensity than that observed in the first 30 min.

The overlapping of the curves after 2 h of exposure indicates a tendency towards stabilization, which may be associated with either the depletion of the most reactive fraction of the pollutant or the partial saturation of the catalyst surface by byproducts.

This behavior is consistent with pseudo-first-order kinetics, in which the reaction rate depends on the residual concentration of the degradable compound.

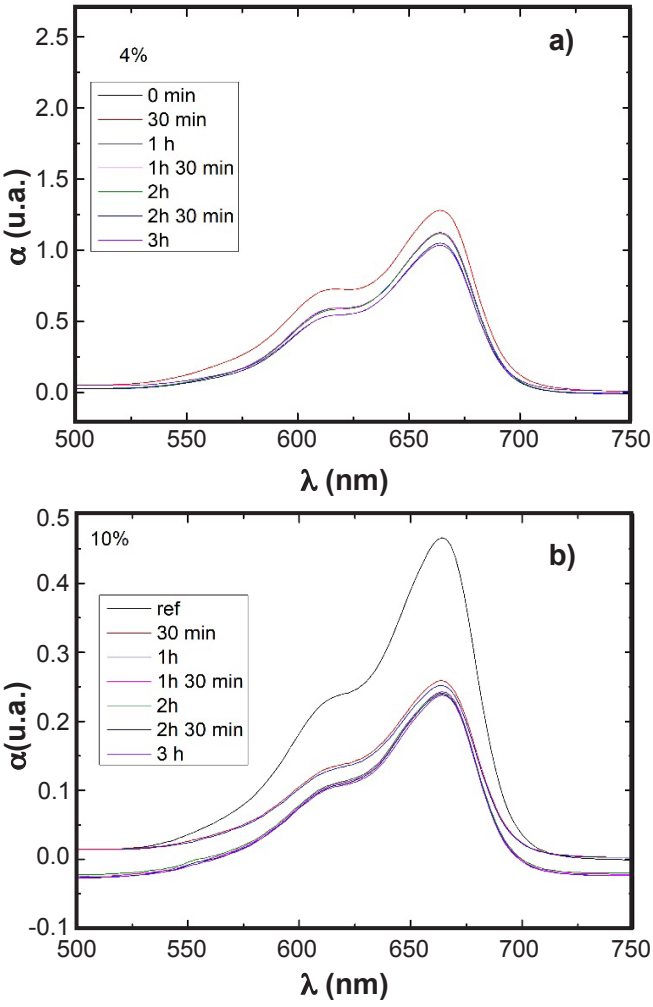

Figure 6 - Absorbance spectra of mortar containing 4% and 6% TiO_2 by cement weight, obtained after different exposure times to ultraviolet radiation.

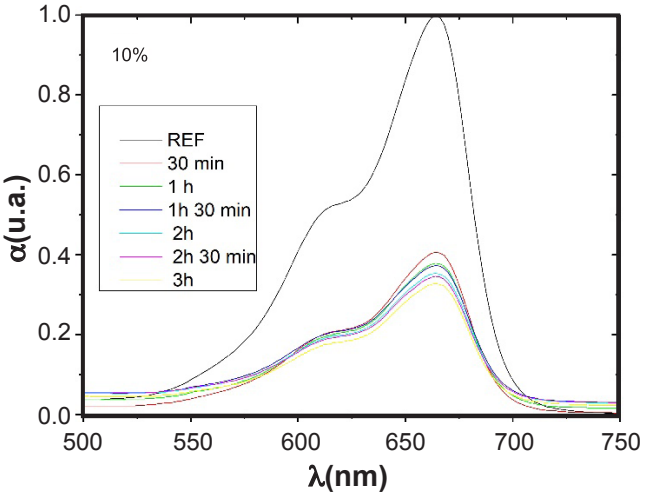

Figure 7: Absorbance spectra of mortar containing 10% TiO_2 by cement weight, obtained after different exposure times to ultraviolet radiation.

Figure 7 shows the absorbance spectra (α, in arbitrary units) as a function of wavelength (λ, in nm) for a mortar sample with 10% TiO_2, subjected to UV radiation for different times: 0, 30 min , 1h, 1h30 min, 2h, 2h30 min, and 3h.

The absorbance spectrum of the mortar containing 10% TiO_2 initially shows a well-defined peak in the reference sample. With exposure over time, a significant reduction in the intensity of the main peak is observed, especially in the region around 650–670 nm, which corresponds to the characteristic absorption band of the monitored dye.

The progressive decrease in absorbance over time demonstrates the photocatalytic degradation of the dye in the presence of TiO_2, attributed to the generation of hydroxyl radicals (•OH) and reactive oxygen species during irradiation.

It is noted that the most pronounced reduction occurs in the first 2 h, indicating a higher initial degradation rate, followed by a tendency to stabilize after 2h30 to 3h, suggesting that a significant portion of the dye had already been degraded. Furthermore, the residual intensity after 3h remains above zero, which may be related to both the presence of intermediate degradation byproducts and the saturation of the photocatalytic capacity of the active surface of TiO_2 at high concentrations.

Figure 8 presents the morphological and compositional characterization of the mortar without the addition of TiO_2 (0%). The micrograph was obtained by Scanning Electron Microscopy (SEM) at 3000x magnification.

A heterogeneous surface is observed, composed of particles of different sizes and shapes, distributed irregularly. This morphology is associated with the cementitious matrix and the hydration products formed, such as hydrated calcium silicate (CSH), in addition to the possible presence of pores and denser regions [21].

Chemical mapping by energy dispersive spectroscopy (EDS) shows the spatial distribution of the predominant elements in the sample. The presence of oxygen (O), silicon (Si), calcium (Ca), aluminum (Al), iron (Fe), magnesium (Mg), and sulfur (S) is noted.

The correlation between these elements confirms the typical composition of the cementitious matrix, mainly composed of calcium and silicon compounds, in addition to oxides from clinker and mineral additions present in the cement.

The EDS spectra confirm the qualitative composition, with characteristic peaks for the detected elements. Strong intensity of the calcium (Ca) and oxygen (O) peaks is observed, consistent with the predominance of hydrated calcium compounds.

According to de Faria e Oliveira Barreto et al. (2024) [21],

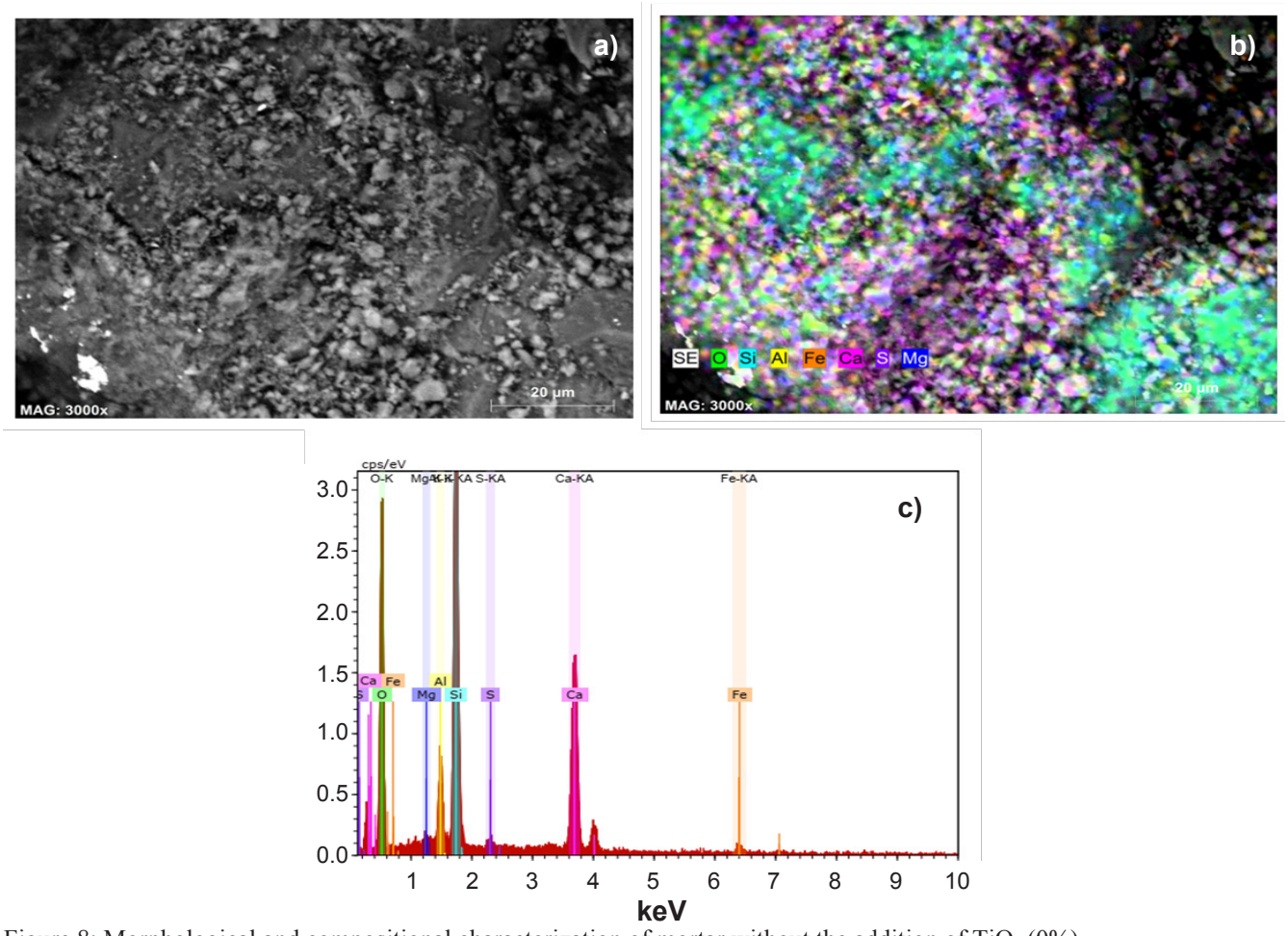

Figure 8: Morphological and compositional characterization of mortar without the addition of TiO_2 (0%).

the element found in the analyzed samples is Ca; this element is present in the composition of the main hydration products of the binders used in the mortars that are the subject of this study (ettringite, portlandite, CSH, and also calcite).

Silicon (Si) appears in significant proportions, originating from the fine aggregate used in large quantities in mortar mixes [21]. The presence of aluminum (Al) and sulfur (S) is associated with the formation of secondary phases, such as aluminum silicate (Al_2SiO_5). Aluminum silicate (Al_2SiO_5) can be linked to metakaolin, a material rich in silica (SiO_2) and alumina (Al_2O_3). In pozzolanic reactions, metakaolin interacts with calcium hydroxide ($Ca(OH)_2$) released during cement hydration, generating aluminosilicate phases, such as hydrated aluminum silicate and other secondary compounds, such as (C–A–S–H) [22].

Iron (Fe) appears in detectable quantities, possibly originating from mineral impurities in the clinker or raw materials used. Magnesium (Mg), although in lower concentration, may be associated with the formation of hydrated magnesium carbonate ($MgCO_3 \cdot H_2O$). This is a secondary phase that forms when magnesium ions (Mg^{2+}) react with carbon dioxide (CO_2) and water (H_2O), especially in humid environments and with exposure to air. This reaction is a form of carbonation, similar to that which occurs with calcium, but involving magnesium [1].

X-ray diffraction (XRD) analysis complements these results, allowing for the crystallographic identification of the phases present.

The following phases were detected: silicon dioxide (SiO_2), calcium carbonate ($CaCO_3$), hydrated magnesium carbonate ($MgCO_3 \cdot H_2O$), aluminum silicate oxide (Al_2SiO_5), and a phase identified as $C_{352.00}$. These phases are consistent with the elements evidenced in the mapping and EDS, confirming that the microstructure of the sample without TiO_2 is composed mainly of calcium and magnesium silicates and carbonates, in addition to secondary phases containing aluminum.

In general, the integrated analysis of SEM, mapping, EDS, and XRD confirms that the sample with 0% TiO_2 presents a typical cementitious mortar composition, with no evidence of the incorporation of the photocatalytic semiconductor.

These results serve as a reference for comparison with the samples modified with TiO_2, allowing for the evaluation of the structural, morphological, and crystallographic changes resulting from the addition of titanium oxide.

Figure 9 presents the morphological and compositional characterization of the mortar containing 2% TiO_2. The micrograph was obtained by Scanning Electron Microscopy (SEM) at 3000x magnification.

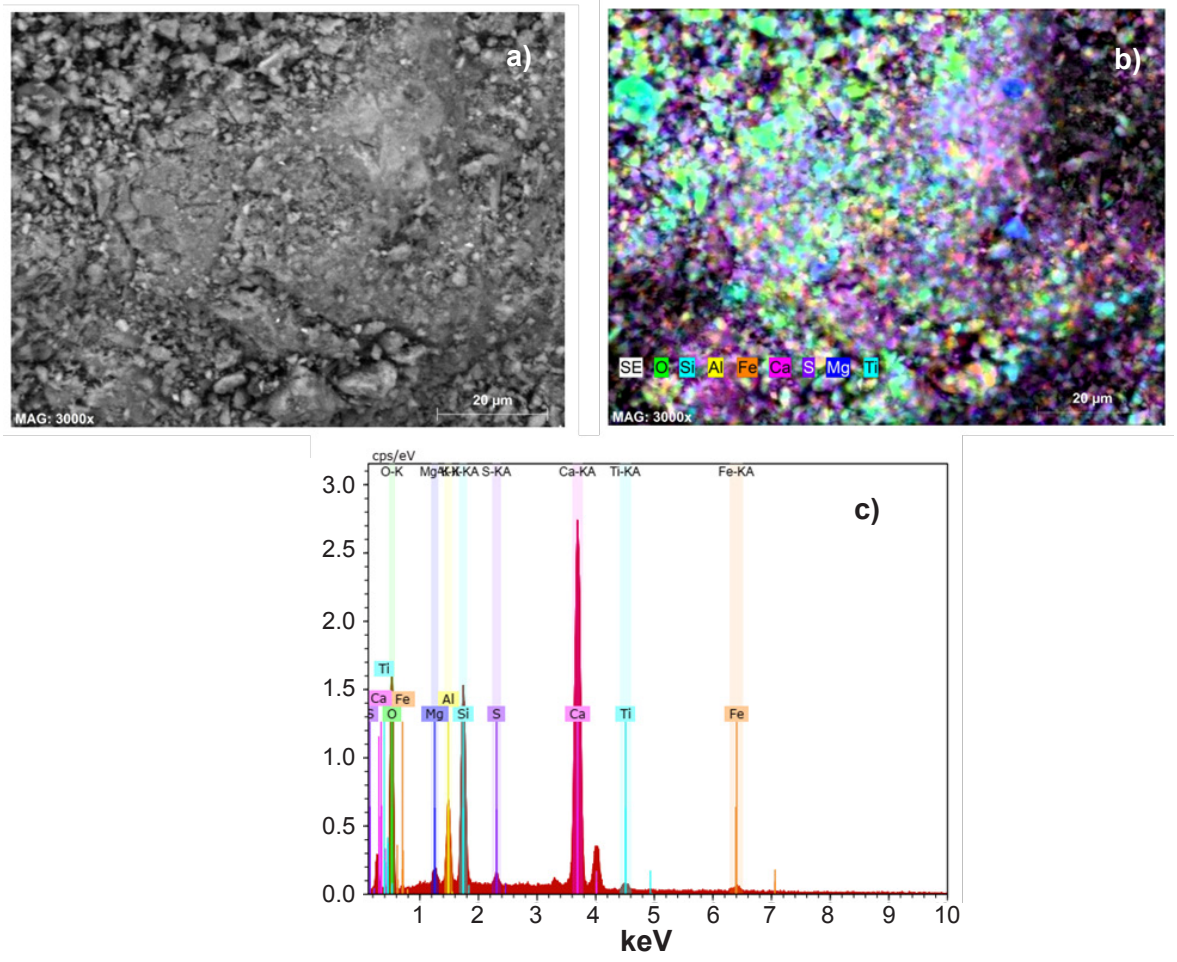

Figure 9: Morphological and compositional characterization of mortar with TiO□ (2%) by cement weight.

The figure reveals a denser and more homogeneous surface compared to the sample without the addition of TiO_2. Improved particle compaction and a more uniform distribution are observed, suggesting that the incorporation of titanium dioxide may have contributed to pore filling and improved cohesion of the cementitious matrix, thus favoring the photocatalytic performance of the material.

Chemical mapping obtained by energy dispersive spectroscopy (EDS) confirms the presence of the main constituent elements of mortar, oxygen (O), silicon (Si), calcium (Ca), and aluminum (Al), in addition to identifying titanium (Ti), evidencing the incorporation of TiO_2 into the matrix.

The homogeneous distribution of this element indicates good dispersion of the photocatalytic additive, an essential factor for maximizing the efficiency of photocatalytic reactions on the mortar surface.

The EDS spectrum shows well-defined peaks for O, Si, Ca, Al, and Ti, with intensities reflecting the relative proportions of these elements. The peak corresponding to titanium (Ti) confirms its effective presence.

Calcium (Ca) and silicon (Si) stand out as the main constituent elements of the sample, with some of the calcium associated with the presence of calcium carbonate ($CaCO_3$), while aluminum (Al) contributes to the formation of secondary phases in the cementitious matrix.

The high intensity of the oxygen signal indicates the predominance of oxides and carbonates in the material's structure, highlighting the oxidized nature of the compounds formed.

X-ray diffraction (XRD) analysis complements and confirms these observations, identifying the predominant crystalline phases in the sample: silicon dioxide (SiO_2), calcium carbonate ($CaCO_3$) or calcite, titanium dioxide (TiO_2), and aluminum silicate (Al_2SiO_5). The presence of the TiO_2 phase confirms the incorporation of the semiconductor into the mortar, in the form of rutile, responsible for the photocatalytic properties. The SiO_2, $CaCO_3$, and Al_2SiO_5 phases are consistent with the typical hydration and reaction products of Portland cement.

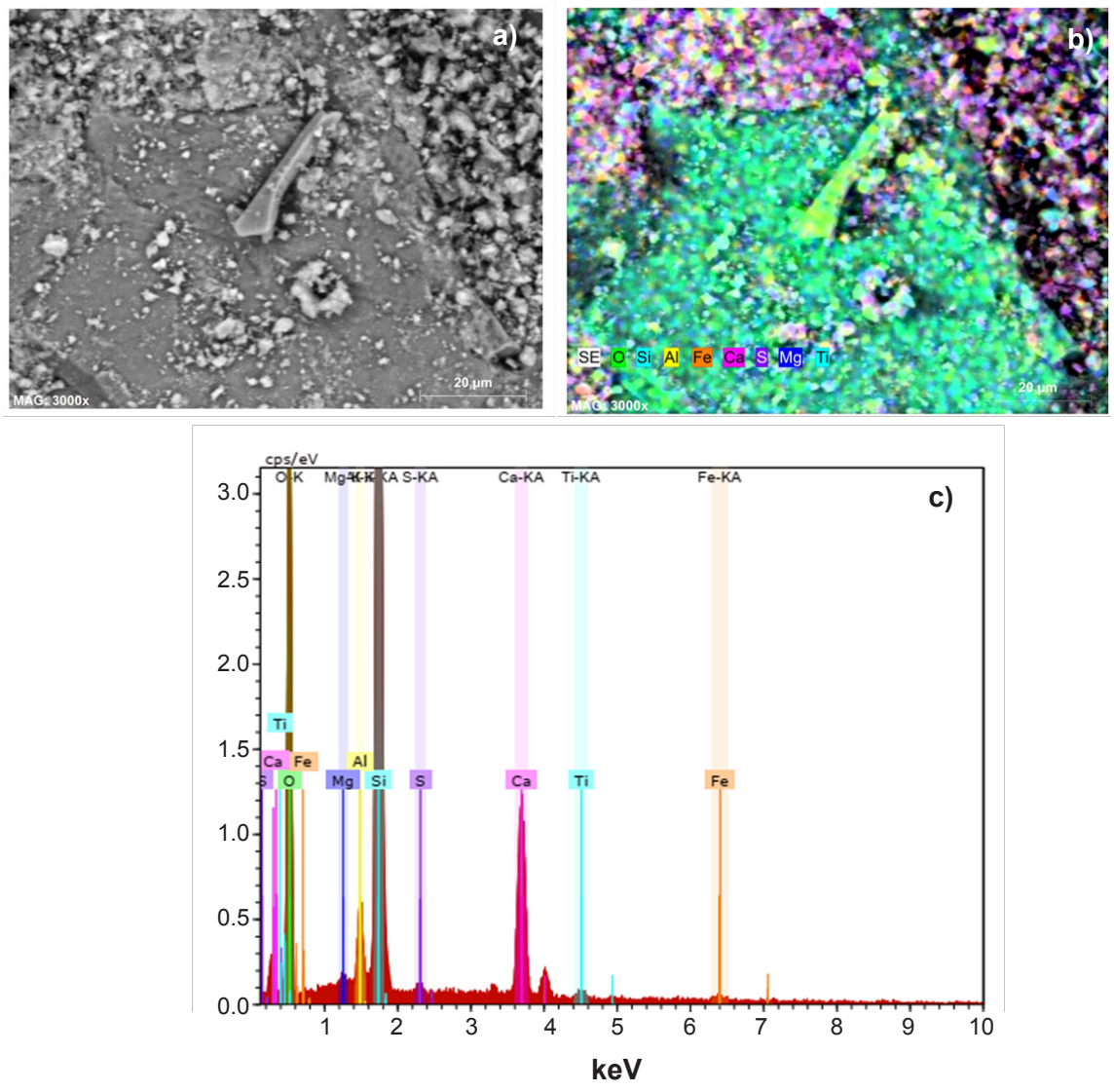

Figure 10: Morphological and compositional characterization of mortar with TiO_2 (4%) by cement weight.

Taken together, the SEM, mapping, EDS, and XRD results show that the addition of 2% TiO_2 promoted significant changes in the mortar microstructure, resulting in a more homogeneous matrix with a uniform distribution of titanium. This microstructural modification is favorable for photocatalytic applications, since it increases the active area exposed to radiation and improves the interaction between TiO_2 and the cementitious matrix.

Figure 10 presents the morphological and compositional characterization of the mortar containing 4% TiO_2. The micrograph was obtained by Scanning Electron Microscopy (SEM) at 3000x magnification.

In the micrograph obtained by Scanning Electron Microscopy (SEM) at 3000x magnification, a relatively compact surface is observed, with well-distributed fine particles and localized agglomeration zones. Compared to the 2% TiO_2 sample, a slight increase in matrix densification and texture homogeneity is noted, indicating that the addition of TiO_2 continues to promote microstructure refinement and reduction of surface porosity [23]. This behavior suggests good integration between the photocatalyst and the cementitious matrix, favoring the continuity of the hydrated phases.

Chemical mapping by EDS confirms the presence of the main elements, oxygen (O), silicon (Si), calcium (Ca), aluminum (Al), and titanium (Ti). Ti is well distributed throughout the analyzed surface, demonstrating satisfactory dispersion of titanium dioxide and indicating that the increase in concentration did not lead to the formation of significant agglomerates.

The overlap of Si- and Ca-rich regions with Ti areas suggests a good interaction between the additive and the matrix, which may contribute to greater microstructure stability and photocatalytic efficiency.

The EDS spectrum shows characteristic peaks of O, Si, Ca, Al, and Ti, with a noticeable intensification of the Ti peak compared to the 2% sample, confirming the increased oxide concentration. Calcium and silicon continue to predominate, and the presence of aluminum remains moderate, reflecting its contribution to the aluminate and aluminosilicate phases.

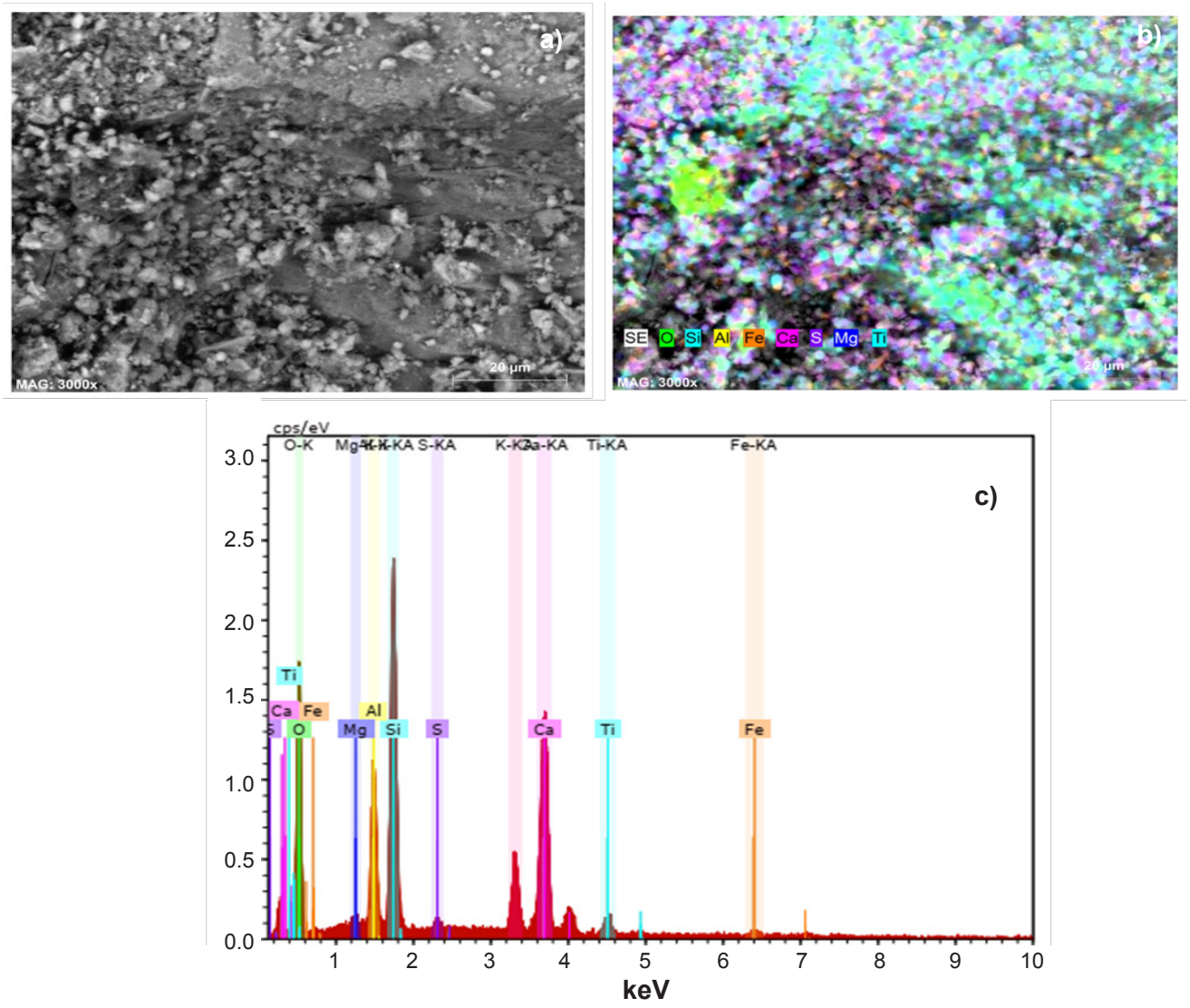

Figure 11: Morphological and compositional characterization of mortar with TiO_2 (6%) by cement weight.

The high oxygen content is related to the presence of oxides and carbonates, typical of the hydrated cementitious matrix.

X-ray diffraction (XRD) revealed the dominant crystalline phases: calcium carbonate ($CaCO_3$), titanium dioxide (TiO_2), silicon dioxide (SiO_2), and aluminum silicate (Al_2SiO_5). The presence of the TiO_2 phase confirms the effective incorporation of the semiconductor into the mortar, while the SiO_2 and $CaCO_3$ phases indicate the continuity of hydration and carbonation reactions. Al_2SiO_5 is related to the presence of aluminosilicates from mineral additions or from the clinker itself.

In general, the integration of SEM, mapping, EDS, and XRD results demonstrates that the sample with 4% TiO_2 presents a compact, homogeneous, and well-distributed microstructure in terms of elemental composition. The addition of TiO_2 in higher concentrations maintains the integrity of the cementitious matrix and reinforces the conditions for photocatalytic activity, representing a balance between adequate dispersion and structural stability.

Figure 11 presents the morphological and compositional characterization of the mortar containing 6% TiO_2. The micrograph was obtained by Scanning Electron Microscopy (SEM) at 3000x magnification.

In the micrograph obtained by Scanning Electron Microscopy (SEM), at 3000x magnification, a surface with a more compact and homogeneous texture is observed, showing a lower incidence of pores and fissures compared to samples with lower TiO_2 content.

The presence of discrete clusters suggests that some of the TiO_2 particles may have concentrated in specific regions, possibly due to the higher quantity of the additive. Even so, the microstructure maintains good cohesion, indicating efficient incorporation of the photocatalyst into the cementitious matrix.

Chemical mapping obtained by energy dispersive spectroscopy (EDS) shows the distribution of the main constituent elements: oxygen (O), silicon (Si), calcium (Ca), aluminum (Al), and titanium (Ti). The mapping confirms

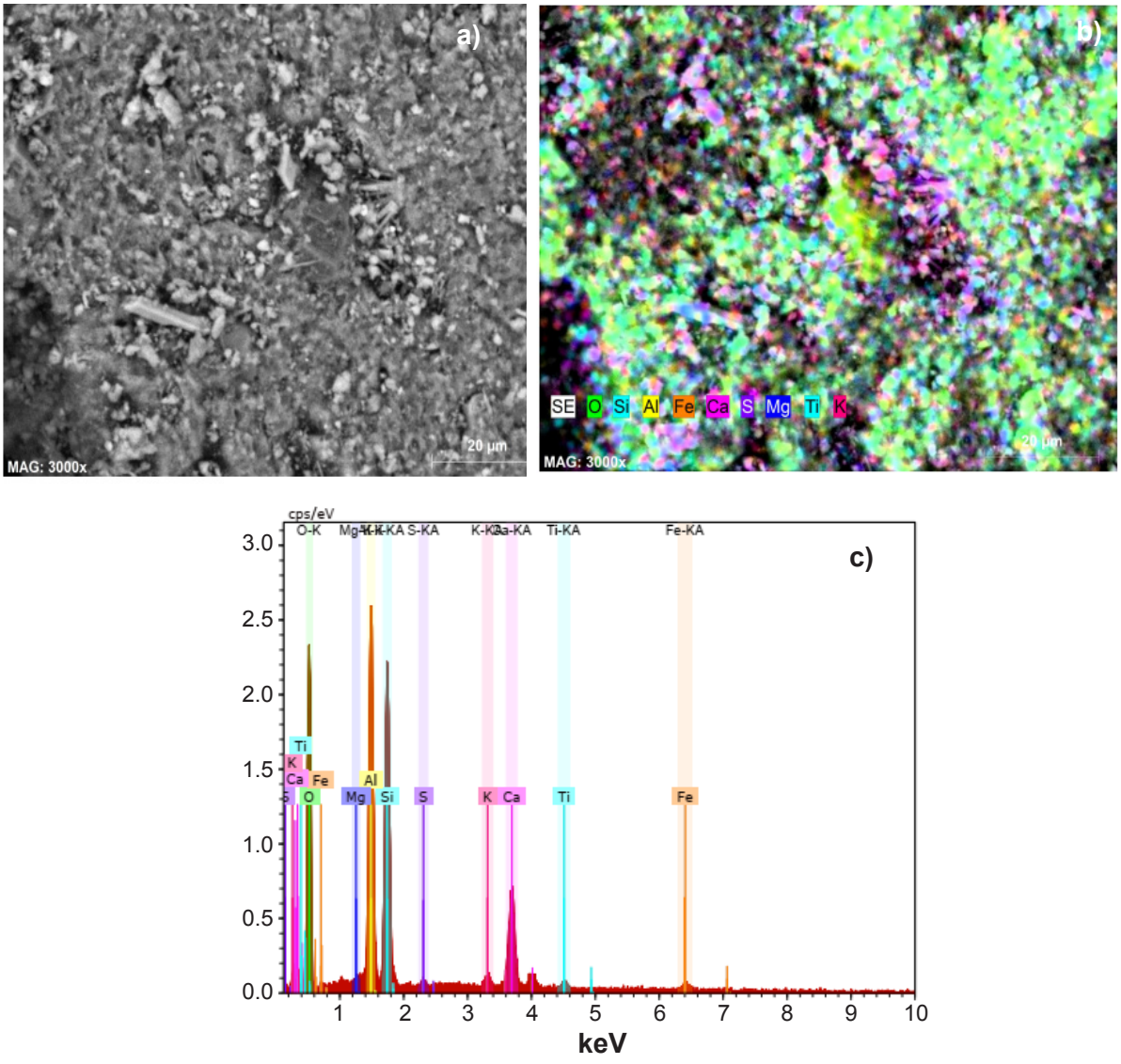

Figure 12:Morphological and compositional characterization of mortar with TiO_2 (10%) by cement weight.

the presence of Ti in a more intense form, consistent with the increased concentration of the oxide in the mixture. The overlapping of regions rich in Ti, Si, and Ca indicates a good interaction between titanium dioxide and the hydration products of the cement, which contributes to increased structural stability and photocatalytic potential of the composite.

The EDS spectrum shows pronounced peaks of O, Si, and Ca, characteristic of cementitious products, in addition to significant peaks of Ti, which become more prominent in this sample compared to previous ones. This increase in Ti intensity confirms the progressive incorporation of titanium dioxide into the matrix, while the Al and Ca peaks remain at levels compatible with the typical phases of aluminates, calcium carbonates, and calcium silicate formed during the hydration and carbonation process.

Calcium silicate ($CaSiO_3$) is one of the main compounds present in cement-based materials, such as mortar. It can be present both as a primary product of cement hydration and as a residual phase of incomplete reactions. In mortar, calcium silicate plays a fundamental role in the mechanical strength and cohesion of the matrix, as it participates in the reactions that form the hydrated compounds responsible for the consolidation of the material. Furthermore, its presence is closely related to the combination of calcium (Ca) and silicon (Si), the major elements of the cementitious matrix, whose interaction results in a predominantly silicate structure.

In microstructural analyses, such as EDS or XRD, the identification of $CaSiO_3$ indicates the occurrence of rearrangements between calcium and silica phases, reflecting the evolution of hydration reactions and/or pozzolanic interactions (in the case of mineral additions, such as metakaolin). This phase contributes to chemical stability and can act as a precursor in the formation of more complex compounds, such as C–S–H (hydrated calcium silicate) [24].

X-ray diffraction (XRD) analysis reinforces the results observed by SEM and EDS, identifying the main crystalline phases of the sample: silicon dioxide (SiO_2), titanium dioxide (TiO)-Brookite, aluminum silicate (Al2SiO), calcium carbonate ($CaCO_3$), and calcium silicate ($CaSiO_3$) The coexistence of these phases evidences the presence of hydration products typical of mortar, as well as the effective incorporation of TiO_2 into the structure.

The TiO_2 phase, possibly in the Brookite form, is responsible for the photocatalytic activity, while the $CaCO_3$ and Ca_2SiO_4 phases reflect the balance between hydration and carbonation. The Brookite phase is a phase of titanium dioxide (TiO_2) that has been shown to exhibit high photocatalytic activity, even surpassing anatase under certain conditions. This activity is attributed to the greater depth of surface electron "traps," which increases the efficiency in separating electron-hole pairs and prolongs the lifetime of the holes, improving photocatalytic performance in various applications [25].

In general, the integration of SEM, mapping, EDS, and XRD results indicates that the sample with 6% TiO_2 presents a more consolidated and titanium-rich microstructure, with good dispersion of the photocatalyst and maintenance of the typical phases of the cementitious matrix. This structural and compositional combination favors photocatalytic performance and may represent an ideal saturation point, at which increasing the TiO_2 content still contributes positively to the uniformity and stability of the material.

Figure 12 presents the morphological and compositional characterization of the mortar containing 10% TiO_2.

In the micrograph obtained by Scanning Electron Microscopy (SEM) at 3000x magnification, a more heterogeneous surface is observed compared to samples with lower TiO_2 content. The increase in oxide content promoted the formation of agglomerates and regions with a higher concentration of fine particles, indicating a possible saturation of the dispersion capacity of TiO_2 in the cementitious matrix. Despite this, the overall structure maintains good cohesion, with dense and compact areas that suggest interaction between the photocatalyst and the hydration products of the cement.

Chemical mapping using energy-dispersive spectroscopy (EDS) reveals the presence of the elements oxygen (O), silicon (Si), calcium (Ca), aluminum (Al), sulfur (S), and titanium (Ti).

The element Ti is identified in greater intensity, confirming the increased quantity added. However, its distribution shows some irregularity, with zones of higher concentration, possibly corresponding to agglomerations of TiO_2 particles. Area's rich in Si and Ca remain predominant, reflecting the basic cementitious structure composed of hydration and carbonation products.

The EDS spectrum shows well-defined peaks of O, Si, Ca, and Ti, with the increased intensity of Ti being direct evidence of greater oxide incorporation. Aluminum (Al) and sulfur (S) appear in proportions consistent with the phases detected by X-ray diffraction (XRD), related to the formation of sulfates and hydrated aluminates. The high intensity of the oxygen peaks reinforces the predominance of oxides and hydroxides, typical of the hydration reactions of Portland cement.

XRD analysis confirms the presence of the main crystalline phases: calcium carbonate ($CaCO_3$), silicon dioxide (SiO_2), calcium hydroxide ($Ca(OH)_2$), titanium dioxide (TiO_2)-Brookite, hydrated aluminum sulfate (Al_2SO_5) $(OH)_4 \cdot H_2O$), and aluminum silicate (Al_2SiO_5). The simultaneous presence of these phases demonstrates the coexistence of cement hydration and carbonation products with the incorporated TiO_2. The TiO_2 phase is responsible for the sample's photocatalytic potential, while $Ca(OH)_2$ and $CaCO_3$ reflect the equilibrium between hydration and carbonation reactions. The hydrated aluminum sulfate phase indicates the formation of secondary products, possibly associated with the interaction between cement and residual sulfate ions. The results indicate that aluminum sulfate can effectively accelerate the setting time of Portland cement and improve the concrete's strength at an advanced age. initial (1 day) [26].

Overall, the integrated analysis of SEM, mapping, EDS, and XRD shows that the sample with 10% TiO_2 has a dense microcrystalline structure, but with evidence of photocatalyst agglomeration.

This condition suggests that an excessive increase in TiO_2 content may partially compromise the uniformity of the dispersion, even while maintaining the chemical integrity of the cementitious matrix. However, a high titanium content ensures greater availability of active sites for photocatalytic reactions, which can improve the mortar's performance in self-cleaning degradation applications.

Figure 13 shows the degradation efficiency (DE), which quantifies the proportion of contaminant removed from the solution during the degradation process for different concentrations of the material used (0%, 2%, 4%, 6%, and 10%).

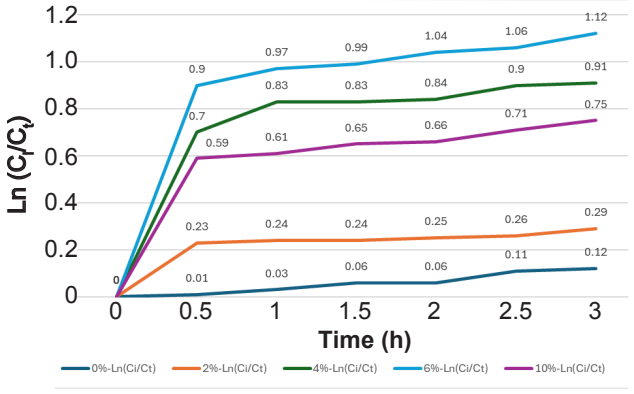

Figure 13: Degradation efficiency (DE) of the contaminant removed from the solution during the degradation process.

It was observed that all samples, except the sample free of TiO_2, showed a significant increase in degradation efficiency in the early stages of the reaction, especially in the first 0.5 h.

This behavior indicates that most of the degradation occurred rapidly at the beginning of the process, possibly due to the high availability of reactive species or radicals responsible for breaking down the contaminant.

After the initial time interval, a tendency towards stabilization of the curves is observed, with smoother variations between 1 and 3 h of reaction. This stabilization may be related to the decrease in the concentration of the residual contaminant and the possible saturation of the catalyst's active sites, or even to the reduction in the intensity of the photochemical reactions over time.

Comparing the different concentrations, it was found that increasing the proportion of the material up to 6% promoted a significant increase in degradation efficiency, reaching a maximum value of 67.29% after 3 h.

However, at 10% there was a reduction in final efficiency (52.79%), suggesting that high concentrations may cause saturation effects, light blocking, or a decrease in the effective contact area between the catalyst and the contaminant.

Samples with lower concentrations showed inferior

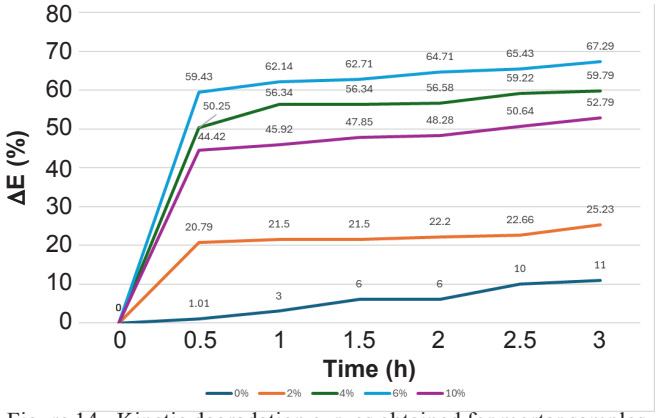

Figure 14 - Kinetic degradation curves obtained for mortar samples containing 0%, 2%, 4%, 6% and 10% TiO□ by cement weight for photocatalytic material.

performance: 4% achieved approximately 59.79% efficiency, while 2% and 0% showed 25.23% and 11%, respectively. The system without additive (0%) showed low degradation, indicating that spontaneous removal of the contaminant is minimal and that the process strongly depends on the presence of the active agent.

In general, the results show that degradation efficiency is higher in the initial stages of the process and that material concentration directly influences performance. Concentrations of 4% and 6% showed the best results, being considered the ideal condition among those studied.

Figure 14 presents the kinetic degradation curves obtained for the mortar samples containing 0%, 2%, 4%, 6%, and 10% photocatalytic material, represented by the variation of $\ln(C_0/Ct)$ as a function of irradiation time (h).

It is observed that the samples containing the photocatalytic material showed a progressive increase in $\ln(C_0/Ct)$ values over time, indicating greater efficiency in contaminant degradation compared to the control sample (0%). The sample without addition (0%) showed practically negligible variation, confirming the absence of photocatalytic activity.

Among the modified samples, it was observed that the degradation kinetics increased up to a certain point with the increase in the percentage of photocatalyst.

The samples with 4% and 6% showed the highest $\ln(C_0/Ct)$ values, indicating a higher rate constant (k) and, therefore, a higher degradation rate.

This improvement is associated with the increased number of active sites available on the particle surface, favoring the generation of reactive species (•OH, $•O^{2-}$) responsible for the oxidation of the contaminant.

On the other hand, it is observed that in the 10% sample, although still higher than the 0% and 2% samples, there is a reduction in the degradation rate compared to the 6% sample.

This behavior can be attributed to the agglomeration effect and the reduction in the efficiency of photocatalyst dispersion in the mortar matrix, which decreases the effective surface area and light penetration.

In general, the results indicate that the degradation kinetics follow a typical behavior of heterogeneous photocatalytic systems, in which there is an optimal concentration of active

material to maximize the efficiency of the process. Thus, the 6% content proved to be the most efficient under the evaluated conditions, presenting the highest value of $\ln(C_0/Ct)$ and, consequently, the highest kinetic degradation coefficient (k).

CONCLUSIONS

Based on the results obtained, it is concluded that the incorporation of titanium dioxide (TiO□) in coating mortars significantly influences both the microstructure and the photocatalytic performance of the material. SEM, EDS, and XRD analyses showed that TiO□ was effectively incorporated into the cementitious matrix, promoting relevant morphological and crystallographic changes. It was observed that increasing the concentration of TiO□ resulted in a denser and more homogeneous matrix up to approximately 6%, at which point the dispersion of the photocatalyst became more balanced.

At higher concentrations (10%), a tendency for agglomeration of TiO_2 particles was observed, which may partially limit the efficiency of the photocatalytic process due to shading between particles and a reduction in the active surface area.

Photocatalysis results demonstrated that all samples containing TiO_2 exhibited photocatalytic activity under UV radiation, with progressive degradation of the methylene blue dye over time. The best performance was observed in the samples with 6% TiO_2, which combined high degradation efficiency with good structural stability. This content proved to be the most suitable for maximizing the balance between dispersion, matrix density, and availability of active sites.

X-ray diffraction analysis confirmed the presence of crystalline phases typical of the cementitious matrix (SiO_2, $CaCO_3$, $Ca(OH)_2$ and Ca_2SiO_4), as well as TiO_2 phases in rutile and brookite forms, responsible for photocatalytic activity. These phases coexist stably, indicating good compatibility between the photocatalyst and the cement hydration products.

In terms of applicability, the developed photocatalytic mortars show great potential for use in facade coatings and exposed surfaces, offering self-cleaning properties.

In addition to aesthetic and functional benefits, these mortars contribute to environmental sustainability by reducing the emission of harmful organic and inorganic compounds and decreasing the need for maintenance and cleaning.

Therefore, the study confirms that the controlled addition of TiO□, especially in the range of 4% to 6%, is an effective strategy for the development of photocatalytic cementitious coatings, promoting the advancement of technologies applied to sustainable civil construction and the development of smart materials aimed at urban well-being.

ACKNOWLEDGMENTS

The authors thank the Federal University of Itajubá (UNIFEI) for the laboratories and technical support, and the company Aditibrás for supplying the superplasticizer mixture. The Article Processing Fee for the publication of this research was funded by the Coordination for the Improvement of Higher Education Personnel - Brazil (CAPES).

DATA AVAILABILITY

The data that support the findings of this study are available from the corresponding author upon reasonable request.

REFERENCES

[1]. B. L. Fontolan, T. B. Silva, G. P. Gava, E. Rigo, A. Neves Junior, e E. Possan, Ambiente Construído **24** (2024), e131131.
[2]. J. D. Bersch, I. Flores-Colen, A. B. Masuero, e D. C. C. D. Molin, Buildings **13** (2023).
[3]. M. Janczarek, Ł. Klapiszewski, P. Jędrzejczak, I. Klapiszewska, A. Ślosarczyk, e T. Jesionowski, Chemical Engineering Journal **430** (2022), 132062.
[4]. E. M. Modan, University of Pitesti. Scientific Bulletin - Automotive Series **29** (2019), 1
[5]. B. L. Fontolan, G. P. Gava, e E. Possan, in *Xix Encontro Nacional De Tecnologia Do Ambiente Construído* (2023), p. 1–12.
[6]. A. H. Navidpour, S. Abbasi, D. Li, A. Mojiri, e J. L. Zhou, Catalysts **13** (2023).
[7]. A. Andaloro, E. S. Mazzucchelli, e A. Lucchini, Journal of Facade Design and Engineering **3** (2017), 1.
[8]. F. Pereira Lessa, O. Lima, É. Margalho, C. Pinheiro, I. Rocha Segundo, e J. Oliveira Carneiro, Journal of Building Pathology and Rehabilitation **10** (2025).
[9]. R. C. Lima da Silva, Research, Society and Development **2022** (2022), 1.
[10]. F. El Koulali, M. Ouzzine, L. Cano-Casanova, M. C. Román-Martínez, e M. A. Lillo-Rodenas, Chemistry of Inorganic Materials **3** (2024), 100059.
[11]. B. P. Resende e F. C. de Faria, Brazilian Journal of Development **8** (2022), 40284.
[12]. ABNT NBR 16697, "Cimento Portland — Requisitos", Ass. Bras. Normas
Técn., Rio Janeiro (2018).
[13]. ABNT NBR 16916, "Agregado miúdo - Determinação da densidade e da absorção de água", Ass. Bras. Normas Técn., Rio Janeiro (2021).
[14]. NBR 16605, "Cimento Portland e outros materiais em pó — Determinação da massa específica", Ass. Bras. Normas Técn., Rio Janeiro (2017).
[15]. ABNT NBR 13279, "Argamassa para assentamento de paredes e revestimento de paredes e tetos - Determinação da retenção de água", Ass. Bras. Normas Técn., Rio Janeiro (1995).
[16]. ABNT NBR 13749, "Revestimento de paredes e tetos de argamassas inorgânicas", Ass. Bras. Normas Técn., Rio Janeiro (2013).
[17]. ABNT NBR7211, "Agregados para concreto - Requisitos", Ass. Bras. Normas
Técn., Rio Janeiro (2022).
[18]. H. El-Diadamony, A. A. Amer, T. M. El Sokkary, e S. El-Hoseny, HBRC Journal **14** (2018), 150.
[19]. K. Weise, N. Ukrainczyk, e E. A. B. Koenders,

Materials; Design **231** (2023).
[20]. C. do Nascimento Fernandes, R. L. S. Ferreira, R. Bernardo, F. Avelino, e A. Bertini, Construction and Building Materials **257** (2020), 119542.
[21]. M. de Faria e Oliveira Barreto, M. R. F. Gontijo, C. P. Teles, e F. F. de Araújo, Revista de Gestão e Secretariado **15** (2024), 01.
[22]. F. C. De Mattos, M. Regina, e F. Gonçalves, Revista Matéria **24** (2019), e-12533.
[23]. F. A. L. W. J. Fleck, E. Polesello, Ambiente Construído **25** (2025), e140806.
[24]. D. Zhao e R. Khoshnazar, Cement and Concrete Composites **122** (2021), 104162.
[25]. G. Žerjav, K. Žižek, J. Zavašnik, e A. Pintar, Journal of Environmental Chemical Engineering **10** (2022), 107722.
[26]. X. Liu, B. Ma, H. Tan, B. Gu, T. Zhang, P. Chen, H. Li, e J. Mei, Construction and Building Materials **232** (2020), 117179.
(Rec. 14-Nov-2025, Rev. 31-Mar-2026, Ac. 30-Apr-2026)
(AE: Daniel Zanetti de Florio)